Exploring the Temperature−Pressure Phase Diagram of Staphylococcal Nuclease†

Gunda Panick,‡ Gediminas J. A. Vidugiris,§ Ralf Malessa,‡ G. Rapp,|| Roland Winter,*,‡ and Catherine A. Royer*,§,⊥

School of Pharmacy, University of Wisconsin−Madison, 425 North Charter, Madison, Wisconsin 53706, Department of Chemistry, Physical Chemistry I, University of Dortmund, Otto-Hahn-Strasse 6, D-44221 Dortmund, Germany, and European Molecular Biology Laboratory, Hamburg Outstation at DESY, D-22603 Hamburg, Germany

Received November 3, 1998; Revised Manuscript Received January 14, 1999

ABSTRACT: The temperature dependence of the pressure-induced equilibrium unfolding of staphylococcal nuclease (Snase) was determined by fluorescence of the single tryptophan residue, FTIR absorption for the amide I′ and tyrosine O−H bands, and small-angle X-ray scattering (SAXS). The results from these three techniques were similar, although the stability as measured by fluorescence was slightly lower than that measured by FTIR and SAXS. The resulting phase diagram exhibits the well-known curvature for heat and cold denaturation of proteins, due to the large decrease in heat capacity upon folding. The volume change for unfolding became less negative with increasing temperatures, consistent with a larger thermal expansivity for the unfolded state than for the folded state. Fluorescence-detected pressure-jump kinetics measurements revealed that the curvature in the phase diagram is due primarily to the rate constant for folding, indicating a loss in heat capacity for the transition state relative to the unfolded state. The similar temperature dependence of the equilibrium and activation volume changes for folding indicates that the thermal expansivities of the folded and transition states are similar. This, along with the fact that the activation volume for folding is positive over the temperature range examined, the nonlinear dependence of the folding rate constant upon temperature implicates significant dehydration in the rate-limiting step for folding of Snase.

In the case of small reversibly folding proteins, the transition between the folded and unfolded conformation(s) can be treated often as a first-order phase transition. We have used such an approach to analyze the pressure-induced unfolding of staphylococcal nuclease (Snase)[1] under various solution conditions, including pH, concentration of denaturant, and concentration of osmolyte, and we have also investigated the kinetic aspects of the unfolding−refolding transitions (*1*−*7*). To describe as thoroughly as possible the ramifications of pressure on the protein's structure, we have observed the pressure denaturation by tryptophan fluorescence emission and histidine ^{1}H NMR (tertiary contacts), peptide carbonyl FTIR (secondary structure), and small-angle X-ray scattering (compactness) both at equilibrium and in pressure-jump relaxation experiments. The results of these studies were consistent with two-state behavior and revealed that the folding reaction involves significant dehydration and collapse of the chain. The unfolded state retains some residual secondary structural characteristics and has a radius of gyration that is more than twice that of the native protein with a bimodal pair probability distribution and a complete disruption of tertiary contacts.

In the early 1970s, Brandts (*8*) and Kauzmann (*9*) explored the temperature−pressure phase behavior of ribonuclease A and metmyoglobin unfolding, respectively. The temperature−pressure dependence of ribonuclease A unfolding has been revisited recently by Jonas and co-workers (*10*), who reported a complete $P-T$ phase diagram based on high-pressure NMR for this protein. A study of the fluorescence-detected pressure denaturation of a destabilized mutant of Snase as a function of temperature was carried out by Eftink and Ramsay (*11*). However, beyond these few studies, there are few examples of thorough pressure−temperature equilibrium thermodynamic studies of protein folding transitions. Moreover, in the above cases where the phase diagram for protein unfolding has been explored, a single observable parameter has been monitored, limiting the global information concerning the structural properties of the denatured states in different areas of the phase diagram. From the few existing studies, it appears that the $P-T$ diagram of proteins is ellipsoidal, with pressure destabilization of proteins at low temperatures and stabilization at high temperatures (see the recent review in ref *12*). However, a deeper understanding of these phenomena requires a much larger database. Thus, in this study, we present the results of the study of the temperature dependence of the pressure-induced unfolding of Snase by fluorescence, FTIR, and SAXS.

† This work was supported by a grant to C.A.R. from the National Science Foundation (MCB9600523) and by a grant from the DFG to R.W.

* To whom correspondence should be addressed. E-mail: winter@steak.chemie.uni-dortmund.de. E-mail: royer@tome.cbs.univ-montp1.fr.

‡ University of Dortmund.

§ University of Wisconsin−Madison.

|| Hamburg Outstation at DESY.

⊥ Current address: Centre de Biochimie Structurale, Faculté de Pharmacie, 15 ave. Charles Flahault, F-34060 Montpellier Cedex 02, France.

[1] Abbreviations: Snase, staphylococcal nuclease; SnaseConA, mutant of Snase bearing a nine-amino acid insert from concanavalin A; FTIR, Fourier transform infrared (spectroscopy); SAXS, small-angle X-ray scattering; NMR, nuclear magnetic resonance; Bis-Tris, 2,2-bis(2-hydroxyethyl)amino-2-(hydroxymethyl)-1,3-propanediol; MOPS, 3-(*N*-morpholino)propanesulfonic acid.

10.1021/bi982608e CCC: $18.00
Published on Web 03/09/1999

MATERIALS AND METHODS

Protein Preparation

Recombinant staphylococcal nuclease (Snase) with the sequence of nuclease A from the V8 strain of *Staphylococcus aureus* was obtained using the λ expression system in the *Escherichia coli* strain Arλ9 as described by Shortle and Lin (*13*). The cells were grown according to the procedure described by Shortle et al. (*14*) except that SB rather than MOPS medium was employed. The protein purification was carried out according to the method described by Shortle and Meeker (*15*) with the modifications described by Frye et al. (*4*). The plasmid bearing the sequence for the V66A mutant was a gift from D. Shortle and was produced and purified as described by Frye and Royer (*6*).

High-Pressure Fluorescence Measurements

The optical pressure cell used in the experiments described here was similar to that previously described (*2, 3*), except that the windows were sapphire and the seal was a C-seal, rather than a Bridgman seal on all plugs. The primary hydraulic pressure was generated by the electric oil-filled pump, followed by use of the pressure intensifier with the intensification ratio of 1:20 and consequent separator for separating primary pressure medium (oil) from the following pressure medium (ethanol). This allowed for attaining higher pressures. After pressure jumps, spectra were acquired every 6−130 s depending upon the relaxation times with an integration time of 6 s. The emission detection system was a back-illuminated UV/VIS (512 pixels × 512 pixels) MTE-CCD detector (Instruments S. A., Inc.) coupled to a Triax-180 Imagining Spectrograph, equipped with the UV blazed double 600/300 g/mm grating (Instruments S. A., Inc.). The CCD detector and Spectrograph were interfaced with the computer by the AT-GPIB/TNT card (National Instruments).

Upon unfolding, emission spectra shifts to the red followed the recorded loss in intensity. Intensity values are those obtained at the weighted average emission wavelength. The protein concentration was approximately 15 μM, and the buffer conditions were 10 mM Bis-Tris at pH 5.5. The temperature was regulated by a programmable temperature controller bath (VWR Scientific model 1157), reacting to the external platinum resistance temperature detector (RTD) probe (Omega Engineering Inc.) placed near the insulated high-pressure cell. The temperature controller bath was coupled to a brass thermostating jacket around the high-pressure cell.

Small-Angle X-ray Scattering

The SAXS experiments were performed at the X13 beamline of the EMBL outstation at DESY in Hamburg (*16, 17*) as previously described (*7*). A protein concentration of 10 mg/mL in 10 mM Bis-Tris was chosen. With this protein concentration, typical exposure times were, due to the window material, 40 min for the pressure-dependent measurements. Pressure release always resulted in recovering of the scattering pattern of the native protein, indicating that no or only minor aggregation or radiation damage occurred during the course of the experiments. The measurements were performed in 10 mM Bis-Tris buffer adjusted to pH 5.5. The cell was thermostated to the appropriated temperature using a temperature jacket and water bath. After subtraction of the background scattering using the pure buffer solution data, taking into account the different absorption factors, we performed data evaluation of the SAXS measurements using the indirect Fourier transformation (*18*−*20*).

We have used SAXS to probe the overall conformation of the protein by measuring its radius of gyration and pair distance distribution function $p(r)$ which are sensitive to the spatial extent and shape of the particle. The square of the radius of gyration R_g of the scattering particle is obtained from the normalized second moment of $p(r)$

$$R_g^2 = \frac{\int_0^{R_{max}} p(r) r^2 \, dr}{2\int_0^{R_{max}} p(r) r \, dr} \quad (1)$$

The pair distance distribution function $p(r)$ is given by the Fourier transform of the measured scattered intensity $I(Q)$

$$p(r) = \frac{1}{2\pi^2}\int_0^{\infty} I(Q) Qr \sin(Qr) \, dQ \quad (2)$$

For a particle with uniform electron density, $p(r)$ is the frequency of vector lengths r connecting small volume elements within the whole volume of the scattering particle with a maximum dimension R_{max}. As a first estimate of the cutoff distances employed in the indirect Fourier transform method of the SAXS analysis for calculation of R_g, $p(r) \approx 0$ and $R_{max} \approx 4R_g$ (with R_g obtained from the Guinier plots) (*21*).

High-Pressure FTIR

High pressure FTIR spectra were recorded with a Nicolet Magna 550 spectrometer equipped with a liquid nitrogen-cooled HgCdTe detector as described previously (*7*). Powdered α-quartz was placed in the hole of the steel gasket, and changes in pressure were quantified by the shift of the quartz phonon band at 695 cm^{-1} (*22*). An external water thermostat was used for pressure- and temperature-dependent measurements to control the temperature within 0.1 °C.

Snase (50 mg) was dissolved in 1 mL of D_2O buffer containing 50 mM Bis-Tris (pH 5.5). The pK_a of Bis-Tris is pressure insensitive since both the acid and base forms exhibit the same charge, thus eliminating electrostriction effects associated with deprotonation. To ensure complete H−D exchange, the protein solution was heated to 40 °C for 1 h and then stored overnight at room temperature.

Fourier self-deconvolution was performed with a resolution enhancement factor of 1.8 and a bandwidth of 15 cm^{-1}. The fractional intensities of the secondary structure elements were calculated from a band-fitting procedure assuming a Gaussian−Lorentzian line shape function (*23*, *24*). Here it is assumed that the transition dipole moments of the different secondary structure elements are similar.

Data Analysis

Equilibrium Profiles. Equilibrium fluorescence intensity and percent helix versus pressure profiles were fit for the Gibbs free energy of unfolding $\Delta G°_u$ and volume change of unfolding $\Delta V°_u$ at atmospheric pressure under the particular solution conditions of each experiment using the BIOEQS software (*25*−*27*) according to eq 3.

$$d(\Delta G^\circ_u)/dp = \Delta V^\circ_u \quad (3)$$

These observable parameters were fit by BIOEQS assuming a two-state model with only folded and unfolded states as populated species.

$$F \rightarrow U \quad (4)$$

where

$$\Delta G^\circ_u(p) = -RT \ln K_{eq}(p) = -RT \ln[[U](p)/[F](p)] \quad (5)$$

The Gibbs free energy and volume change parameters are adjusted using a Levenberg−Marquardt nonlinear least-squares algorithm until the minimum χ^2 value is attained. Observable mapping is carried out by assigning an adjustable fluorescence intensity plateau value to both the folded and unfolded states. Thus, each fit involves four adjustable parameters: the Gibbs free energy at atmospheric pressure, the volume change of unfolding, and the plateau intensity values. Raw data were fit, and then the data and the fits were normalized to the recovered plateau values for comparison. Uncertainty on the recovered parameters was estimated by carrying out rigorous confidence limit testing of the recovered parameters, a process in which the fit is repeated at each one of a series of tested parameter values, allowing all other parameters in the fit to float. In this manner, the estimated error takes into account the correlation between fitting parameters and is more realistic than errors derived from the diagonal of the correlation matrix.

Relaxation Profiles and Kinetic Parameters. Fits of the relaxation profiles for the relaxation time τ were carried out assuming a simple single-exponential process

$$I(t) = I_o e^{-t/\tau} + C \quad (6)$$

where $I(t)$ is the fluorescence intensity value at time t, I_o is the intensity at time zero, and C is the asymptotic value at any given pressure.

The dependence of the natural logarithm of the inverse of the relaxation time upon pressure was fit to a two-state transition between the folded and unfolded monomer. Since the extent of the perturbation of the equilibrium due to the pressure jump itself was less than 10%, and since we assume a simple two-state model, the linearized rate expression in eq 7 for a simple monomer unfolding reaction holds (*28*).

$$\tau(p) = 1/[k_f(p) + k_u(p)] \quad (7)$$

where $k_f(p)$ and $k_u(p)$ correspond to the rate constants of folding and unfolding at pressure p, respectively. The variation of the rate constants of folding and unfolding with pressure is expressed in terms of their values at atmospheric pressure (k_{of} and k_{ou}) and the activation volumes for the folding and folding reactions $\Delta V^\ddagger_f$ and $\Delta V^\ddagger_u$, respectively

$$k_f(p) = k_{of} e^{[-p(\Delta V^\ddagger_f)/RT]} \quad (8)$$

and

$$k_u(p) = k_{ou} e^{[-p(\Delta V^\ddagger_u)/RT]} \quad (9)$$

Plots of $\ln[1/\tau(p)]$ versus pressure were fit by substituting eqs 8 and 9 into eq 7 and taking natural logarithms.

$$1/\tau(p) = k_{of} e^{[-p(\Delta V^\ddagger_f)/RT]} + k_{ou} e^{[-p(\Delta V^\ddagger_u)/RT]} \quad (10)$$

Constrained analysis was performed using eq 11 which takes into account the relationships between the rate constants and equilibrium constants (eqs 12 and 13). In this manner, only two parameters were adjustable in the fits (k_{of} and $\Delta V^\ddagger_f$), while the values for K_{eqf} and ΔV°_f were fixed at the values obtained from the fits of the equilibrium profiles.

$$1/\tau(p) = k_{of} e^{[-p(\Delta V^\ddagger_f)/RT]} + [k_{of} e^{[-p(\Delta V^\ddagger_f)/RT]}]/[K_{eqf} e^{[-p(\Delta V^\circ_f)/RT]}] \quad (11)$$

The rate constants and activation volumes for unfolding and folding are related to the Gibbs free energy and equilibrium volume change of unfolding through the following relations:

$$\Delta G^\circ_u = -RT \ln K_{equ} = RT \ln(k_{of}/k_{ou}) \quad (12)$$

and

$$\Delta V^\circ_u = \Delta V^\ddagger_u - \Delta V^\ddagger_f \quad (13)$$

RESULTS AND DISCUSSION

Temperature Dependence of the Fluorescence-Detected Equilibrium Pressure Unfolding. Equilibrium fluorescence-detected pressure-induced unfolding profiles of Snase at five different temperatures are shown in Figure 1. The lines through the points represent fits to the data to a simple two-state unfolding transition as described in Materials and Methods, and the recovered values for the Gibbs free energy and volume change of unfolding ΔG°_u and ΔV°_u, respectively, can be found in Table 1. The profile of the Gibbs free energy change ΔG°_u of unfolding obtained from the fluorescence profiles as a function of temperature is shown in Figure 5a. The nonlinear behavior can be ascribed to the well-known increase in heat capacity upon unfolding and has been observed previously for the temperature dependence of the pressure denaturation of a mutant of this protein, SnaseconA (*11*). The cold denaturation of Snase at atmospheric pressure has been reported previously as well (*29*). The studies of Eftink and Ramsay actually were carried out prior to our understanding of the large positive activation volume involved in folding of Snase (*2*) which necessitates quite long equilibration periods. For example, complete equilibration at 2 °C required up to 3 h at each pressure point (see below) and the present estimates of ΔG°_u and ΔV°_u are probably a bit more accurate than those previously published by ourselves and others (*1*, *11*). Moreover, the previous temperature studies (*11*) involved a mutant and not the wild type protein. The overall trend in the Gibbs free energy as a function of temperature is similar to the results of the previous studies on SnaseconA, although the wild type protein is shown here (as expected) to be more stable. The recovered values of the volume changes as a function of temperature are shown in Figure 6a (▲). We note that the error is significantly larger at low temperatures because the extremely long equilibration times (>3 h/pressure point) precluded collecting a large number of points. And since the reported error bars correspond to errors calculated from rigorous confidence limit testing, the correlation between Gibbs free energy and volume change and the asymptotic

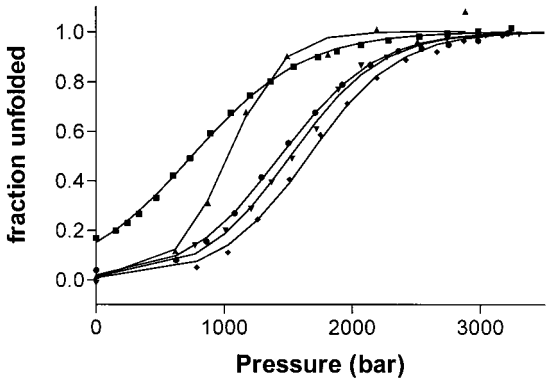

FIGURE 1: Fluorescence-detected equilibrium unfolding profiles for Snase at (▲) 2, (▼) 10, (◆) 21, (●) 30, and (■) 40 °C. Lines through the points represent fits to the data according to eqs 1 and 3 as described in Materials and Methods. Raw intensity data and the fits were normalized to the recovered values for the high- and low-pressure intensity plateaus and plotted as the fraction unfolded for direct comparison. Conditions were as described in Materials and Methods as well.

Table 1: Equilibrium Unfolding Parameters for Snase from the Fluorescence-Detected High-Pressure Experiments[a]

T (°C)	$\Delta G°_u$ (kcal/mol)	$\Delta V°_f$ (mL/mol)	T (°C)	$\Delta G°_u$ (kcal/mol)	$\Delta V°_f$ (mL/mol)
2	2.6 ± 1.0	90 ± 15	30	2.1 ± 0.2	58 ± 6
10	3.2 ± 1.0	84 ± 10	40	1.2 ± 0.1	52 ± 4
21	3.2 ± 0.6	70 ± 10			

[a] Uncertainty values were determined from rigorous confidence limit testing as described in Materials and Methods.

intensity values is quite large. Nonetheless, it is clear from inspection of Figure 6a that increasing temperature results in a decreasing value for the volume change for folding $\Delta V°_f$. The trend is roughly linear, and the slope of the linear fit of $\Delta V°_f$ versus temperature is -1 mL mol^{-1} deg^{-1}. This slope corresponds to $\Delta\alpha_f$, which is the change in the coefficient of thermal expansion upon folding (*9*). This indicates, not surprisingly, that the thermal expansivity of the partial molar volume of the unfolded state is larger than that of the folded state. It also provides an explanation for the change in sign in the volume change of unfolding at high temperatures. In fact, the phase diagrams for metmyoglobin published by Kauzmann (*9*) exhibit curvature at high temperatures and low pressures such that the volume change for unfolding becomes positive. Such behavior can be explained by the difference in thermal expansivities of the folded and unfolded states. Since the partial molar volume of the unfolded state increases more significantly with temperature than that of the folded state, the difference in volume between the two states must decrease with increasing temperature, first tending toward zero and then changing sign (see the schematic diagram in Figure 9).

Temperature Dependence of the Equilibrium FTIR and SAX Profiles. The pressure and temperature dependence of the infrared absorption by the tyrosine O−H stretch and the amide I′ bands of Snase and of a less stable mutant of Snase which we have previously studied V66A (*6*) was investigated using the high-pressure FTIR diamond anvil cell previously described (*7*). Examples of the results at 20 °C are shown in Figure 2. The band corresponding to the tyrosine O−H stretch and that of the amide I′ absorption for both the V66A mutant and wild type (WT) Snase exhibit a transition as a

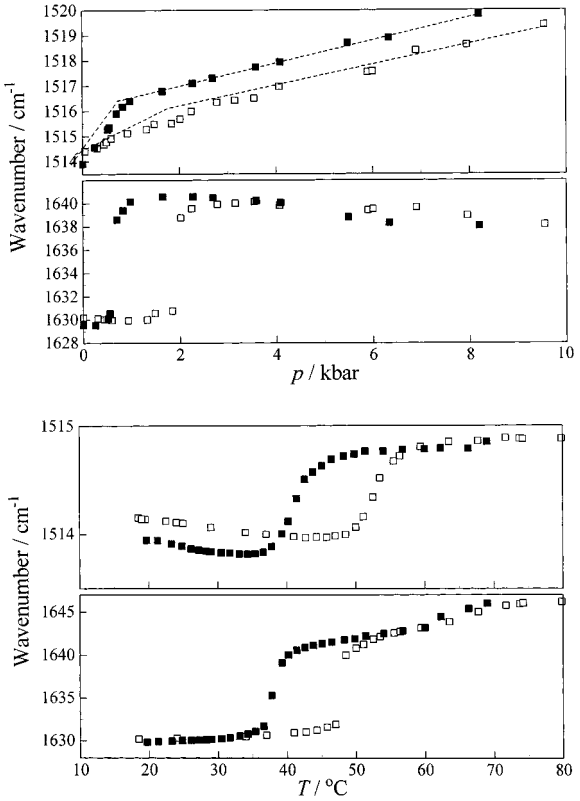

FIGURE 2: Pressure−temperature FTIR results for Snase (□) and Snase V66A (■). (Top panel) Shift in the maximum of the tyrosine O−H (1514−1520 cm^{-1}) and (next panel) amide I′ (1630−1640 cm^{-1}) absorption band maxima as a function of pressure at 25 °C. (Bottom two panels) Shift in the maximum of the tyrosine O−H (1514−1520 cm^{-1}) and amide I′ (1630−1640 cm^{-1}) absorption bands as a function of temperature at atmospheric pressure. Conditions were as described in Materials and Methods.

function of pressure (top two panels). The linear increase in frequency for the O−H stretch at high pressures is due to a direct effect of pressure on the O−H bond. The amide I′ band at each pressure and temperature was analyzed by Fourier self-deconvolution as described in Materials and Methods. The decrease in α-helix and β-sheet content and the concomitant increase in the content of random coil structures as a function of pressure at 20 °C are shown for V66A and WT Snase, respectively, in panels a and b of Figure 3. The loss of secondary structure confirms that the pressure-induced transition corresponds to unfolding of the protein. The values of $\Delta G°_u$ and $\Delta V°_u$ recovered from fits of these data in terms of a two-state unfolding transition can be found in Table 2 and are plotted in Figures 5a (■) and 6a (■), respectively.

In Figure 4 are plotted the values of the radius of gyration R_g for Snase as a function of pressure at 25, 45, and 60 °C obtained from the Guinier analysis of the small-angle X-ray scattering profiles as described in Materials and Methods. Both temperature and pressure lead to an increase in R_g. Compared to the effect of temperature alone, which resulted in R_g values of near 45 Å (*7*), even a small amount of pressure at 60 °C results in a smaller value of R_g (37 Å). The pressure midpoints at several temperatures obtained from the FTIR, SAXS, and fluorescence profiles of WT Snase are plotted as a phase diagram in Figure 5b.

The phase diagram obtained from the FTIR measurements on the V66A less stable mutant is also shown. It can be seen

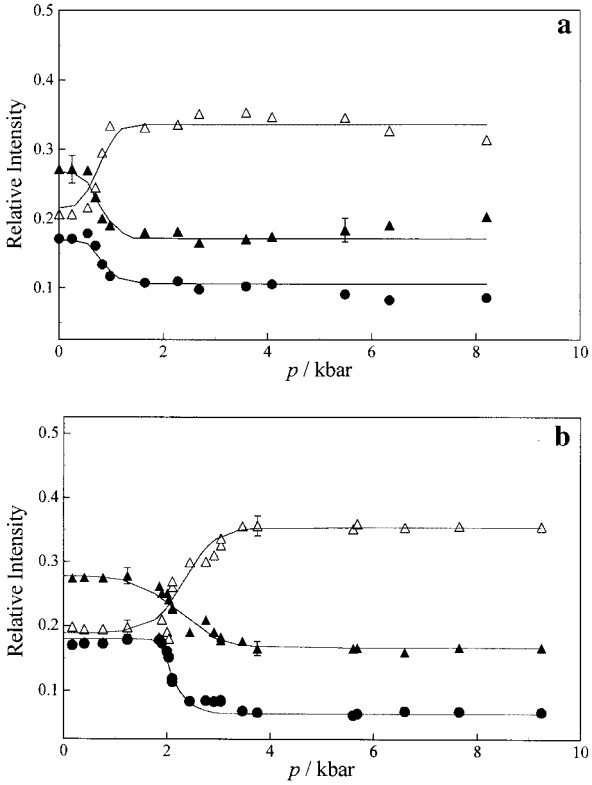

FIGURE 3: Relative fractional intensities of (●) α-helix, (▲) β-sheet, and (△) random coil structures at 25 °C as a function of pressure for (a) V66A and (b) WT Snase calculated from Fourier self-deconvolution of the pressure dependence of the amide I′ absorption band as described in Materials and Methods. Conditions were as described in Materials and Methods.

Table 2: Equilibrium Unfolding Parameters for Snase from the FTIR-Detected High-Pressure Experiments

T (°C)	$\Delta G°_u$ (kcal/mol)	$\Delta V°_f$ (mL/mol)	T (°C)	$\Delta G°_u$ (kcal/mol)	$\Delta V°_f$ (mL/mol)
−4.5	2.0 ± 0.75	92 ± 20	20.0	4.6 ± 1.7	80 ± 20
0.5	2.2 ± 0.9	90 ± 20	25.0	4.0 ± 1.6	77 ± 20
5.0	3.0 ± 1.5	87 ± 20	36.0	3.1 ± 1.1	67 ± 20
10.0	4.15 ± 1.7	87 ± 25	40.0	2.1 ± 0.8	55 ± 25
15.0	4.5 ± 1.7	84 ± 20	45.0	0.61 ± 0.5	35 ± 15

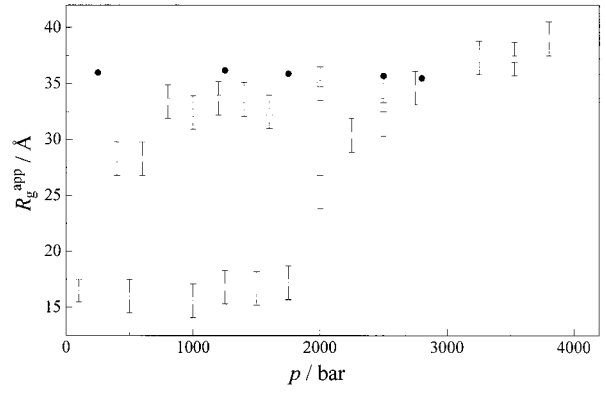

FIGURE 4: Radius of gyration of WT Snase as a function of pressure at (×) 25, (□) 45, and (●) 60 °C, calculated from Guinier analysis of the low-angle scattering profiles. Conditions were as described in Materials and Methods.

that all of the phase diagrams exhibit the curvature typical of heat and cold denaturation of proteins. The data from the FTIR and SAXS measurements for WT Snase are in good

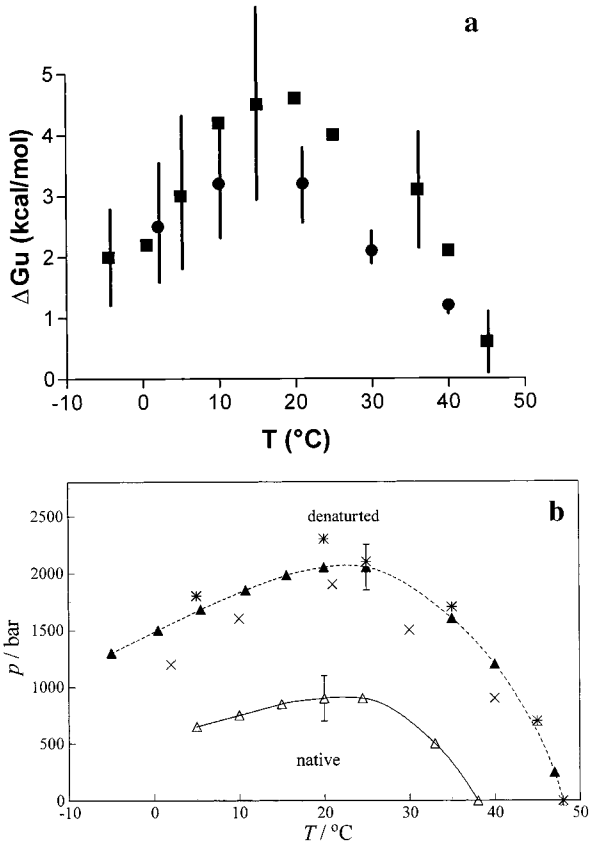

FIGURE 5: Temperature dependence of the volume changes for Snase folding determined from the fluorescence-detected equilibrium and kinetic profiles as described in Materials and Methods. (a) $\Delta G°_u$, the equilibrium Gibbs free energy change upon unfolding (●) determined from fluorescence and (■) determined from FTIR, and (b) the $T-P$ phase diagram of Snase as detected by (*) SAXS with WT Snase, (▲) FTIR with WT Snase, and (△) FTIR with Snase V66A and (▲) WT Snase. Error bars correspond to the one standard deviation of the data as determined from rigorous confidence limit testing of the recovered parameters, and include uncertainty due to correlations between fitting parameters.

agreement, whereas those obtained from the fluorescence profiles indicate that the protein is slightly less stable than one would conclude from the FTIR and SAXS measurements; however, individually the measurements are all within experimental error. Moreover, the values are much less well determined for the SAXS and FTIR measurements than for the fluorescence measurements (see the uncertainties in Tables 1 and 2). We cannot rule out the possibility that the small deviation between fluorescence and FTIR and SAXS represents a breakdown of the two-state behavior under pressure. However, in atmospheric pressure experiments, the fluorescence and CD denaturant unfolding profiles of Snase are identical (*15*), and all of the data we have taken under pressure by fluorescence, FTIR, and SAXS at equilibrium and kinetically are consistent with a reversible two-state transition. One difference between the experimental conditions for fluorescence and FTIR and SAXS that cannot be avoided is that fluorescence measurements are carried out using approximately 15 μM Snase, while the detection limits of the high-pressure FTIR and SAXS measurements require much higher protein concentrations, in the millimolar range. It could be that at the higher protein concentrations, interactions between Snase monomers lead to a small degree of stabilization.

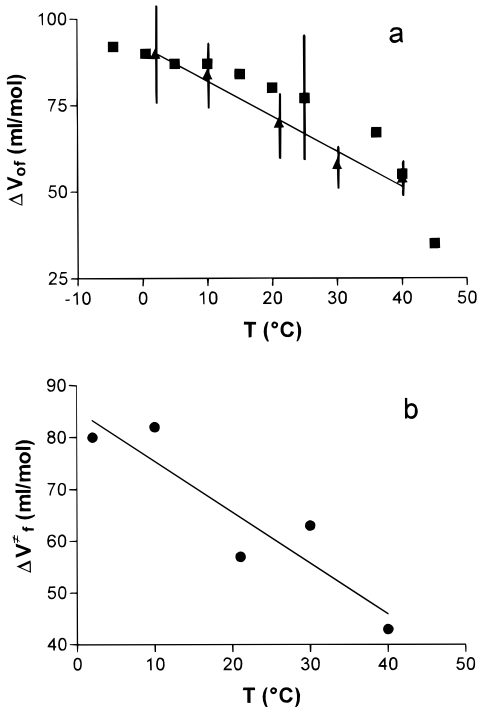

FIGURE 6: Temperature dependence of the volume changes for the folding of Snase. (a) Equilibrium volume change for folding $\Delta V°_f$ as determined from the (▲) fluorescence-detected and (■) FTIR-detected profiles. The line represents a linear regression of the values determined from the fluorescence data. (b) Activation volumes for folding as determined from the fluorescence-detected pressure-jump relaxation profiles. The slopes of the linear regression of the two plots which are the change in thermal expansivity of Snase upon folding $\Delta\alpha_f$ are the same within error and are equal to -1 mL mol^{-1} deg^{-1}.

Temperature Dependence of the Fluorescence-Detected Pressure-Jump Unfolding and Refolding Relaxation Kinetics. Fluorescence-detected pressure-jump relaxation profiles were obtained as a function of pressure at five different temperatures and fitted to single-exponential decay functions as described previously (*2*, *6*). Plots of the inverse of the relaxation time $1/\tau$ as a function of pressure at five temperatures can be found in Figure 7a−e. The data were fit according to eq 8 (Materials and Methods) for the activation volumes and rate constants for folding and unfolding. The values for the activation volumes and rate constants for unfolding are not uniquely determined by the data in an unconstrained analysis. We have previously reported a small positive activation volume for unfolding from linear fits of the data (*2*). In fact, nonlinear fits reveal that the effect of pressure on the unfolding reaction is so small that it does not provide a large enough perturbation to uniquely determine its effects. If we constrain the fit (eq 9) using the equilibrium volume change for folding and the equality between the ratio of the rate constants and the equilibrium constant (Table 1), then the uncertainty for the parameters for folding (activation volume and rate constant at atmospheric pressure) is greatly reduced. And the parameters for unfolding can then be calculated using the above-mentioned relations. These values are given in Table 3.

We note that the trend for the unfolding rate constant is the same and also the numbers quite similar, regardless of the fit method. On the other hand, the constrained analysis allows for the calculation of unfolding constants from the reasonably well-determined equilibrium and folding kinetic parameters. As previously found at 21 °C, we find here a relatively large positive activation volume for folding, consistent with a rate-limiting step for folding involving significant dehydration. Plots of the natural logarithm of the rate constants for folding and unfolding at atmospheric pressure as a function of inverse temperature can be found in Figure 8a,b. It can be seen that similar nonlinear behavior is observed for the natural logarithm of the rate constant for folding and for the equilibrium Gibbs free energy change of unfolding (Figure 5a). Such non-Arrhenius behavior of the natural logarithm of the folding rate constant with temperature has been previously observed in other systems (*30*) and has been interpreted as implicating a large decrease in heat capacity and thus, the extent of dehydration, in the rate-limiting step of the folding reaction. Recent isostability studies implicate the heat capacity change upon formation of the transition state, rather than a fundamental non-Arrhenius dependence of the folding reaction (*31*). Due to the paucity of points, we have not fit the plot for the value of the heat capacity change between the unfolded and transition states, $\Delta C_{pf}^{\ddagger}$, since its value would be highly underdetermined.

The temperature dependence of the activation volume for folding (Figure 6b) is quite similar to the decrease in the value of the equilibrium volume change upon folding (Figure 6a) with increasing temperature. This indicates that the coefficient for thermal expansion of the unfolded state is larger than that of the transition state which is itself quite similar to that of the folded state (see the schematic diagram in Figure 9).

As can be seen from Figure 7b, the relationship between the natural logarithm of the rate constant for unfolding and the inverse kelvin temperature is linear. Following Eyring (*32*) and later Oliveberg et al. (*30*), we have assumed a quasi-thermodynamic equilibrium between the unfolded and activated or transition state. In such a case, one can extract the enthalpy and entropy of activation for unfolding from the plot of the $\ln(k_{ou}/T)$ versus $1/T$.

$$k_{ou} = \frac{k_b T}{h} e^{-\Delta G^{\ddagger}/RT} \tag{14a}$$

$$k_{ou}/T = (k_b \kappa/h) e^{(\Delta S^{\ddagger}/R)} e^{(-\Delta H^{\ddagger}/RT)} \tag{14b}$$

Thus, the intercept of the plot in Figure 8b is $\ln(k_b\kappa/h) + \Delta S^{\ddagger}/R$, and the slope is $-\Delta H^{\ddagger}/R$. Assuming a transmission coefficient κ of 1, we recover an entropy of activation $\Delta S^{\ddagger}$ equal to 227 J mol^{-1} K^{-1} (or 54 eu) and an enthalpy of activation $\Delta H^{\ddagger}$ of 36 kcal/mol. If the transmission coefficient tends toward zero, then the value of the activation entropy doubles. Thus, the entropy of the activated state is higher than that of the folded state. This can be understood because the chain entropy has likely increased due to the breaking of internal tertiary interactions, but no loss in the solvent entropy has occurred since the transition state is not yet highly hydrated like the unfolded state. The enthalpy also increases upon going from the folded to the activated state, which is also consistent with the disruption of tertiary contacts.

CONCLUSIONS

In recent years, a number of investigators (*30*, *31*, *33*−*39*) have applied multiple perturbations (temperature, dena-

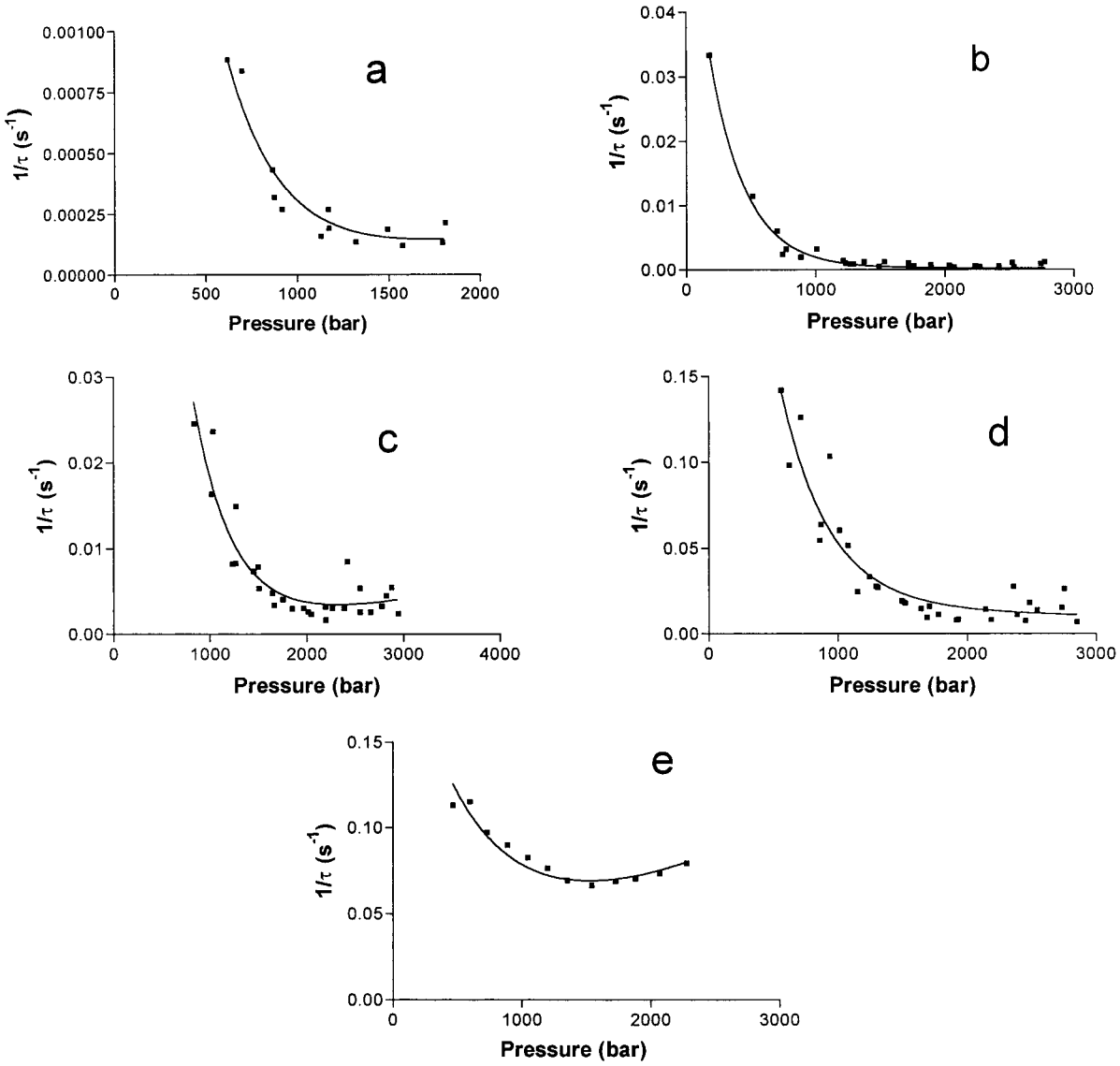

FIGURE 7: Plots of $1/\tau$ vs pressure for Snase at (a) 2, (b) 10, (c), 21, (d) 30, and (e) 40 °C. Lines through the points represent fits to the data using eq 9. Values of τ (the relaxation time) were obtained from fits of the relaxation profiles at each pressure and temperature (data not shown) according to eq 4. Conditions were as described in Materials and Methods.

Table 3: Kinetic Unfolding Parameters from the Fluorescence-Detected Pressure-Jump Relaxation Experiments

T (°C)	k_{of} (s^{-1})	$\Delta V°_f$ (mL/mol)	k_{ou}[a] (s^{-1})	$\Delta V°_u$[a] (mL/mol)
2	0.007 ± 0.001	80 ± 5	0.00006	−10
10	0.062 ± 0.002	82 ± 3	0.0002	−2
21	0.178 ± 0.024	57 ± 3	0.0007	−23
30	0.51 ± 0.06	63 ± 3	0.0154	9
40	0.194 ± 0.007	43 ± 1	0.281	−11

[a] Analysis was carried out as described in the text, constraining the value of the unfolding rate constant k_{ou} to be equal to the ratio of the folding rate constant and the equilibrium constant for folding. The values for K_{eqf} and the ΔV_{eqf} were fixed at the values recovered from the fits of the equilibrium fluorescence data at each temperature. Thus, only fitting parameters were the rate constant for folding at atmospheric pressure k_{of} and the activation volume for folding $\Delta V^{\ddagger}_f$.

turant, osmolytes, and pH) to small reversibly folding proteins and have applied to the data a two-state analysis which corresponds to a first-order phase transition. The general result of these studies has been that the data in so many different dimensions actually correspond reasonably well to this simple picture. Within the limits of practicality, we have presented here the results of simultaneous exploration of the temperature and pressure axes using observables for tertiary structure, secondary structure, and degree of collapse. This study and the others on Snase pressure unfolding (vs pH and GuHCl and osmolyte concentration, and observed using multiple order parameters for secondary structure, tertiary contacts, and collapse) all generally concord to provide a picture of the transition state that lies closer to the folded than the unfolded state in terms of system volume, heat capacity, exposed surface area, and thermal expansivity. This leads to the conclusion that the rate-limiting step in folding corresponds to dehydration and collapse. Our pressure−temperature studies on Snase, and recent isostability temperature dependence studies by Scalley and Baker (*31*) on protein L, provide food for thought to those proponents of the "new view" or energy landscape perspective of protein folding (*40*). Both the pressure and temperature dependencies of the folding reaction explicitly implicate desolvation in the barrier to the folding reaction, whereas this process is only implicit in the contact models; the correspondence between real proteins folding and these models remains to be described in detail.

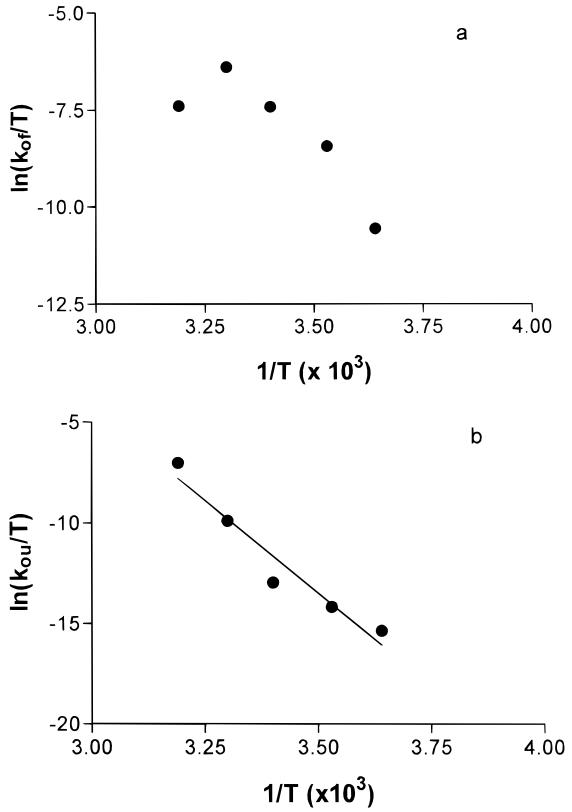

FIGURE 8: Temperature dependence of the rate constants for (a) folding k_{of} and (b) unfolding k_{ou} at atmospheric pressure recovered from fits of the data in Figure 7. The plots are Eyring plots, and the line through the points in panel b represents a linear regression of these data with a slope of -18.4 ± 2.7 and an intercept of 51 ± 9.

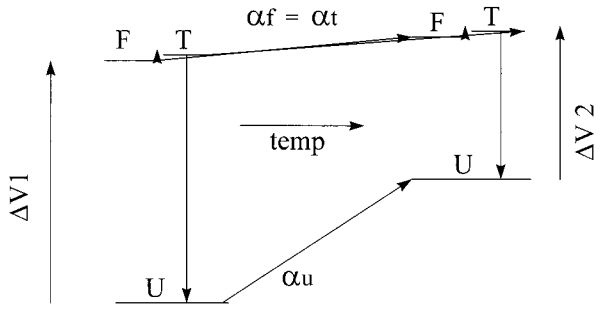

FIGURE 9: Schematic diagram of the effect of temperature on the partial specific volumes of the folded and unfolded states. Since the coefficient of thermal expansion for the folded state α_f is smaller than that of the unfolded state α_u, the decrease in volume upon unfolding becomes smaller in absolute value as the temperature is increased, eventually reaching zero and changing sign, as noted by Kauzmann (*9*).

REFERENCES

1. Royer, C. A., Hinck, A. P., Loh, S. N., Prehoda, K. E., Peng, X., Jonas, J., and Markley, J. L. (1993) *Biochemistry 32*, 5222−5232.
2. Vidugiris, G. J. A., Markley, J. L., and Royer, C. A. (1995) *Biochemistry 34*, 4909−4912.
3. Vidugiris, G. J. A., Truckses, D. M., Markley, J. L., and Royer, C. A. (1996) *Biochemistry 35*, 3857−3864.
4. Frye, K. J., Perman, C. S., and Royer, C. A. (1996) *Biochemistry 35*, 10234−10239.
5. Frye, K. J., and Royer, C. A. (1997) *Protein Sci. 6*, 789−793.
6. Frye, K. J., and Royer, C. A. (1998) *Protein Sci. 7* (in press).
7. Panik, G., Malessa, R., Winter, R., Rapp, G., Frye, K. J., and Royer, C. A. (1998) *J. Mol. Biol. 275*, 389−402.
8. Brandts, J. F., Oliveira, R. J., and Westort, C. (1970) *Biochemistry 9*, 1038−1047.
9. Zipp, A., and Kauzmann, W. (1973) *Biochemistry 12*, 4217−4228.
10. Zhang, J., Peng, X., Jonas, A., and Jonas, J. (1995) *Biochemistry 34*, 8631−8641.
11. Eftink, M. R., and Ramsay, G. D. (1996) in *High-Pressure Effects in Molecular Biophysics and Enzymology* (Markley, J. L., Northrop, D. B., and Royer, C. A., Eds.) pp 62−73, Oxford University Press, New York.
12. Heremans, K., and Smeller, L. (1998) *Biochim. Biophys. Acta 1386*, 353−370.
13. Shortle, D., and Lin, B. (1985) *Genetics 110*, 539−555.
14. Shortle, D., Meeker, A. K., and Gerring, S. L. (1989) *Arch. Biochem. Biophys. 272*, 103−113.
15. Shortle, D. (1986) *J. Cell. Biochem. 30*, 281−289.
16. Rapp, G. (1992) *Acta Phys. Pol. A82*, 103−120.
17. Czeslik, C., Malessa, R., Winter, R., and Rapp, G. (1996) *Nucl. Instrum. Methods Phys. Res., Sect. A 368*, 847−851.
18. Glatter, O. (1977) *Acta Phys. Austriaca 47*, 83−102.
19. Glatter, O. (1979) *J. Appl. Crystallogr. 12*, 166−175.
20. Glatter, O., and Kratky, O. (1982) in *Small-angle X-ray scattering*, Academic Press, New York.
21. Müller, K., and Glatter, O. (1982) *Makromol. Chem. 183*, 465−479.
22. Siminovitch, D. J., Wong, P. T. T., and Mantsch, H. H. (1987) *Biochemistry 26*, 3277−3287.
23. Byler, D. M., and Susi, H. (1986) *Biopolymers 25*, 469−487.
24. Prestrelski, S. J., Byler, D. M., and Liebman, M. N. (1991) *Biochemistry 30*, 133−143.
25. Royer, C. A., Smith, W. R., and Beechem, J. M. (1991) *Anal. Biochem. 191*, 287−294.
26. Royer, C. A., and Beechem, J. M. (1992) *Methods Enzymol. 210*, 481−493.
27. Royer, C. A. (1993) *Anal. Biochem. 210*, 91−97.
28. Eigen, M., and De Maeyer, L. (1963) in *Relaxation Methods in Techniques in Organic Chemistry* (Weissberger, A., Ed.) pp 895−1054, Wiley, New York.
29. Griko, Y. V., Privalov, P. L., Sturtevant, J. M., and Venyaminov, S. Y. (1988) *Proc. Natl. Acad. Sci. U.S.A. 85*, 3343−3347.
30. Oliveberg, M., Tan, Y.-J., and Fersht, A. R. (1995) *Proc. Natl. Acad. Sci. U.S.A. 92*, 8926−8929.
31. Scalley, M. L., and Baker, D. (1997) *Proc. Natl. Acad. Sci. U.S.A. 94*, 10636−10640.
32. Gladstone, S., Laidler, K. J., and Erying, H. (1941) *The theory of rate processes*, McGraw-Hill, New York.
33. Otzen, D. E., Itzhaki, L. S., ElMasry, N. F., Jackson, S. E., and Fersht, A. R. (1994) *Proc. Natl. Acad. Sci. U.S.A. 91*, 10422−10425.
34. Itzhaki, L. S., Otzen, D. E., and Fersht, A. R. (1995) *J. Mol. Biol. 254*, 260−288.
35. Matoushek, A., Otzen, D. E., Itzhaki, L. S., Jackson, S. E., and Fersht, A. R. (1995) *Biochemistry 34*, 13656−13662.
36. Prieto, J., Wilmans, M., Juménez, M. A., Rico, M., and Serrano, L. (1997) *J. Mol. Biol. 268*, 760−778.
37. Scalley, M. L., Yi, Q., Gu, H., McCormack, A., Yates, J. R., III, and Baker, D. (1997) *Biochemistry 36*, 3373−3382.
38. Dalby, P. A., Oliveber, M., and Fersht, A. (1998) *Biochemistry 37*, 4674−4679.
39. Plaxco, K. W., Guijarro, J. I., Morton, C. J., Pitkeathy, M., Campbell, I. D., and Dobson, C. M. (1998) *Biochemistry 37*, 2529−2537.
40. Onuchic, J. N., Luthey-Schulten, Z., and Wolynes, P. G. (1997) *Annu. Rev. Phys. Chem. 48*, 545−600.

BI982608E